Microscopic four-cluster description of the mirror nuclei ^{9}Li and ^{9}C

K. Varga,[1,2] Y. Suzuki,[3] and I. Tanihata[1]
[1]*RIKEN, Hirosawa, Wako, Saitama 351-01, Japan*
[2]*Institute of Nuclear Research of the Hungarian Academy of Sciences, Debrecen, P.O. Box 51, H-4001, Hungary*
[3]*Physics Department, Niigata University, Niigata 950-21, Japan*
(Received 8 November 1994; revised manuscript received 24 May 1995)

The ^{9}C and ^{9}Li mirror nuclei are studied in a microscopic $\alpha+{}^3\mathrm{He}+p+p$ and $\alpha+{}^3\mathrm{H}+n+n$ four-cluster model using the stochastic variational method. The ^{7}Be-^{7}Li and ^{8}B-^{8}Li mirror subsystems are also investigated with the same effective interaction. The calculated ground-state energies, the radii, and the densities of the nucleons are in good agreement with the experimental data. The magnetic and quadrupole moments, except for the magnetic moments of ^{8}B and ^{8}Li, are also reproduced well. The quadrupole moments of ^{9}C and ^{7}Be are predicted to be -5.04 e fm^2 and -6.11 e fm^2. A possibility of the existence of neutron (proton) halo structure is studied.

PACS number(s): 21.60.Gx, 21.45.+v, 27.20.+n

I. INTRODUCTION

The experimental and theoretical investigations of the neutron- and proton-rich light unstable nuclei attract wide attention due to their unique "halo" structures. To cope with the formidable difficulty imposed by the nonuniform density distribution of these nuclei we developed a microscopic multicluster model comprising $0s$-shell clusters. In our approach [1] the wave function is an antisymmetrized product of the internal states of the clusters and the functions of the relative motions. Various cluster arrangements are combined to include the different correlations between the clusters. The function of the relative motion is approximated by a linear combination of nodeless harmonic-oscillator functions of different size parameters. To keep the dimension of the basis low, we apply the stochastic variational method (SVM) [1,2], in which we select the "important" basis states by using an admittance test. This procedure was successfully tested and applied to the neutron-rich helium isotopes [1,3] and also to five- and six-body systems [4].

This paper, inspired by the recently accumulated new experimental data and by the rapid development of theoretical models, is devoted to the theoretical study of the ^{9}C and ^{9}Li mirror nuclei in the $\alpha+h+p+p$ and in the $\alpha+t+n+n$ four-cluster framework ($h\equiv{}^3\mathrm{He}$ and $t\equiv{}^3\mathrm{H}$). Their most important $^8\mathrm{B}=\alpha+h+p$ and $^8\mathrm{Li}=\alpha+t+n$ three-cluster and $^7\mathrm{Be}=\alpha+h$ and $^7\mathrm{Li}=\alpha+t$ two-cluster (mirror) subsystems are also investigated. The most important experimental stimulations for this study include (1) recent measurements of interaction cross sections and the deduced radii, and (2) the measurement of the magnetic moment of ^{9}C and the planned measurement of ^{9}C quadrupole moment [5].

The structures of ^{7}Be and ^{7}Li are quite successfully described by $\alpha+h$ and $\alpha+t$ two-cluster models [6–8]. More recently, due to the possible proton halo of ^{8}B [9,10] and to the astrophysical interest, various three-cluster models [11–14] have been developed for ^{8}B and ^{8}Li nuclei. The four-cluster model of ^{9}Li and ^{9}C formed by adding one nucleon to the three-body systems seems to be a natural extension of these models. This description automatically includes the $^8\mathrm{Li}+n$, $^7\mathrm{Li}+n+n$ and $^6\mathrm{He}(=\alpha+n+n)$ plus t cluster decompositions of ^{9}Li and the corresponding mirror decompositions of ^{9}C.

To understand the exotic nature of ^{11}Li, various $^9\mathrm{Li}+n+n$-type three-body models have been used [15–17]. These models assume a simple passive ^{9}Li core. This picture is certainly oversimplified and therefore the investigation of the structure of ^{9}Li is necessary to understand the halo phenomena of ^{11}Li.

Our treatment is unified: The same effective two-nucleon (sum of central and spin-orbit) force is applied to the two-, three-, and four-cluster systems and the same configuration space is used for the mirror pairs; that is, the mirror systems differ only in the Coulomb interaction. We calculate the ground-state energies, the radii of the proton, neutron, and matter distributions, and the magnetic and quadrupole moments. To explore the halo structure, the nucleon density distributions and the one- and two-nucleon spectroscopic amplitudes are also calculated.

The plan of this paper is as follows. In Sec. II we give a brief outline of our formalism. The microscopic multicluster model is defined in Secs. II A and II B. Section II C is devoted to demonstrating the efficiency and accuracy of the SVM. Section III contains the results of the calculations. The input parameters and angular momentum channels are discussed in Secs. III A and III B. The relative importance of various arrangements is shown in Sec. III C by calculating the so-called amount of clustering. Energies, radii, and magnetic and quadrupole moments are compared with experiment in Sec. III D. Section III E discusses density distributions and the halo structure. In the last section we discuss the results and summarize the most important conclusions.

II. FORMALISM

A. Microscopic multicluster model

In this subsection we briefly sketch our formalism. A more exhaustive treatment is given elsewhere [1,4]. To describe the system of interacting clusters of nucleons, we

build up a trial function which is a sum over the various cluster arrangements μ (see Fig. 1), each associated with a particular set of intercluster Jacobi coordinates $\boldsymbol{\rho}_1^\mu, \ldots, \boldsymbol{\rho}_{n-1}^\mu$. The spins s_i of the clusters are coupled to S, and the orbital angular momenta $l_i \equiv l_i^\mu$ belonging to the Jacobi coordinates $\boldsymbol{\rho}_i^\mu$ are coupled to L. The wave function of the intercluster motion is approximated by a linear combination of nodeless harmonic-oscillator functions (or "Gaussians") of different size parameters:

$$\Gamma_{l_i m_i}(\nu_{k_i}^\mu, \boldsymbol{\rho}_i^\mu) = G_{l_i}(\nu_{k_i}^\mu) \exp[-\nu_{ik}^\mu (\rho_i^\mu)^2] \mathscr{Y}_{l_i m_i}(\hat{\boldsymbol{\rho}}_i^\mu), \quad (1)$$

with

$$G_l(\nu) = \left[\frac{2^{2l+7/2} \nu^{l+3/2}}{\sqrt{\pi}(2l+1)!!} \right]^{1/2}, \quad \mathscr{Y}_{lm}(\mathbf{x}) = x^l Y_{lm}(\hat{\mathbf{x}}), \quad (2)$$

where ν_{ik}^μ is the kth size parameter of the ith relative motion in the cluster arrangement μ.

The wave function belonging to an arrangement μ and angular momenta $[(s_1, \ldots, s_n)S, (l_1, \ldots, l_{n-1})L]JM$ can be written as

$$\Psi^\mu_{[(s_1,\ldots,s_n)S,(l_1,\ldots,l_{n-1})L]JM} = \sum_K C^\mu_{K,(s_1,\ldots,s_n)S(l_1,\ldots,l_{n-1})L} \mathscr{A}\{[\Phi_{(s_1,\ldots,s_n)S} \Gamma^\mu_{K(l_1,\ldots,l_{n-1})L}(\boldsymbol{\rho}_1^\mu, \ldots, \boldsymbol{\rho}_{n-1}^\mu)]_{JM}\}, \quad (3)$$

where $\mathscr{A}$ is the intercluster antisymmetrizer and $\Phi_{(s_1,\ldots,s_n)SM_S}$ is a vector-coupled product of the intrinsic wave function of the clusters. The intrinsic wave functions are constructed from harmonic-oscillator Slater determinants with size parameter β, and the intrinsic function for single nucleons is just their spin function. The function $\Gamma^\mu_{K(l_1,\ldots,l_{n-1})L}(\boldsymbol{\rho}_1^\mu, \ldots, \boldsymbol{\rho}_{n-1}^\mu)$ is a vector-coupled product of the intercluster relative functions $\Gamma_{l_i m_i}(\nu_{k_i}^\mu, \boldsymbol{\rho}_i^\mu)$, where K stands for the set of the indices $\{k_1, \ldots, k_{n-1}\}$ of the size parameters. The sequence of angular momentum coupling is chosen so as to follow the pattern of the Jacobi coordinates. By using an integral transformation [4], the antisymmetrized product in Eq. (3) can be rewritten as a linear combination of Slater determinants of Gaussian wave packet single-particle functions. The matrix elements between Slater determinants of these nonorthogonal single-particle states are evaluated analytically by using the algebraic manipulation language MATHEMATICA [18].

The variational trial function is a combination of different arrangements and intercluster angular momenta:

$$\Psi = \sum_\mu \sum_{(s_1,\ldots,s_n)S} \sum_{(l_1,\ldots,l_{n-1})L} \Psi^\mu_{[(s_1,\ldots,s_n)S,(l_1,\ldots,l_{n-1})L]JM}. \quad (4)$$

We give a detailed form of the wave function in Appendix A for the three-cluster case to guide the reader.

B. Cluster arrangements

The description of the $\alpha+h+n+n$ four-body dynamics is obviously nontrivial. In a variational framework one has to find suitable trial functions to approximate the wave function of the system. One possible way is to choose a particular Jacobi arrangement (different Jacobi coordinate systems, "cluster arrangements," are shown in Fig. 1) and to decompose the wave function into a complete set of partial waves in this Jacobi coordinate system. The convergence of energy with inclusion of higher partial waves is, however, rather slow as will be shown later (see also [19]). This might be the consequence of the fact that the description of different types of correlations between the particles in a given Jacobi coordinate system requires the inclusion of higher partial waves, and that the contribution of higher partial waves to the asymptotic part of the wave function is important. Both effects are expected to be important in loosely bound halo nuclei.

The partial waves in a given cluster arrangement form a complete set of states and the different Jacobi coordinate systems are, therefore, equivalent. The components $\Psi^\mu_{[(s_1,\ldots,s_n)S,(l_1,\ldots,l_{n-1})L]JM}$ and $\Psi^{\mu'}_{[(s_1,\ldots,s_n)S',(l_1',\ldots,l_{n-1}')L']JM}$ in the cluster arrangements μ and μ' are, however, rather different: Any component $\Psi^\mu_{[(s_1,\ldots,s_n)S,(l_1,\ldots,l_{n-1})L]JM}$ in a particular arrangement can only be represented by an infinite sum in terms of another arrangement. The relation of partial wave components of different cluster arrangements is shown in Appendix B for a simple case.

The second possibility is to (1) decompose the wave function into partial waves in a given Jacobi coordinate system, (2) truncate the higher partial waves, and (3) complete the wave function by inclusion of low partial waves of different Jacobi arrangements [see Eq. (4)]. This is the basic principle of the coupled-rearrangement-channels method [20] and it is widely used in cluster model calculations [12–14].

Each set of Jacobi coordinates implies a particular asymptotic configuration and emphasizes a particular type of cor-

TABLE I. Energies of two-, three-, and four-nucleon systems interacting via the Volkov potential [21].

System	Method	Energy (MeV)
$2N$	Numerical integration	-0.545
	SVM	-0.545
$3N$	Faddeev equation [19]	-8.43
	SVM: (12)3, $l_1=l_2=0$	-8.00
	SVM: (12)3, $l_1=l_2\leq 4$	-8.38
	SVM: (12)3+1(23) $l_1=l_2=0$	-8.25
	SVM: $(3N)$=(12)3+1(23)+2(13) $l_1=l_2=0$	-8.46
	SVM: $(3N)$=(12)3+1(23)+2(13) $l_1=l_2\leq 2$	-8.46
$4N$	Hyperspherical harmonics [22]	-30.40
	SVM: $(2N)+(2N)$, $l_1=l_2=l_3=0$	-29.17
	SVM: $(3N)+N$, $l_1=l_2=l_3=0$	-29.27
	SVM: $(3N)+N$, $l_1+l_2+l_3\leq 2$	-29.41
	SVM: $[(2N)+(2N)]+[(3N)+N]$, $l_1=l_2=l_3=0$	-30.42
	SVM: $[(2N)+(2N)]+[(3N)+N]$, $l_1+l_2+l_3\leq 2$	-30.42

relations. Our experience is that, to describe the motion of the system for short distances, it is enough to choose a few states in any of the arrangements, and those provide a major part of the total binding energy. However, it is very difficult to describe the "asymptotic" region belonging to one arrangement by a basis that conforms to another arrangement, and that is why it is useful to include several arrangements, even if these asymptotic regions do not contribute to the binding very much. For example, one cannot expect a perfect description of a separation of ^{9}Li into (αt) and (nn) by a truncated basis of the form of $((\alpha t)n)n$, and that is what is improved by the inclusion of a set of functions of the form of $(\alpha t)(nn)$.

C. Stochastic variational method

The numerous possible arrangements and angular momenta combined with the size parameters in the expansion make the dimension of the basis prohibitively large. These basis functions are, however, nonorthogonal and not all of them are equally important. In a previous paper [1] we tested different methods to select the parameters ν_{ik}^{μ} that span most adequately the state space, while the dimension of the basis is kept feasible. The most efficient procedure found is the following [4]. We generate size parameter sets by random choice from a region which is physically important. The parameter sets that satisfy an admittance condition are selected as basis states. Let us assume that N basis states are already selected and the energy in this N-dimensional basis is E_N. Then we admitted a candidate if it, together with the previously selected basis states, lowers the energy more than a preset value ε:

$$E_{N+1}<E_N-\varepsilon. \tag{5}$$

To avoid being trapped on flat plateaus by this condition, we decrease ε dynamically during the search. The angular momentum channels and cluster arrangements are also randomly chosen.

If $\kappa=25$ successive candidates fail to fulfill the condition [Eq. (5)], we divide ε by 2 and continue the search. The starting value is $\varepsilon=0.25$ MeV in the present calculation and the search is terminated at $\varepsilon=0.25/2^8$ MeV$\approx$0.001 MeV. The parameters ε and κ control the rate of convergence. The present values have been found to give reliable solutions and economical calculations: Too big ε and κ might further reduce the size of the basis, but then more matrix elements have to be calculated and/or the basis will not be reliable enough, while too small values may lead to the acceptance of a great number of unimportant basis states. Each calculation was repeated several times to check the convergence. This procedure gives excellent numerical convergence in energy and reduces the number of trial terms considerably.

We present a test example in order to show the accuracy and effectiveness of the SVM and to establish that the inclusion of cluster arrangements is needed for an accurate solution of the dynamics of a multiparticle system. For this purpose we solve two-, three-, and four-nucleon problems using a simple spin-independent Volkov interaction [21] defined as

$$V(r)=144.86e^{-1.487r^2}-83.34e^{-0.3906r^2}(\text{MeV}). \tag{6}$$

As several calculations using this potential are available, we can compare the solutions by the SVM to those of other methods available in the literature. For the two-nucleon system ($L=0$) we used five basis functions with different widths.

To illustrate the role of the combination of the cluster arrangements, we consider the case of three-nucleon system by treating the nucleons as distinguishable particles. Denoting the nucleons as 1 (neutron with spin up), 2 (neutron with spin down), and 3 (proton with spin up), we have three Jacobi arrangements (12)3, 1(23), and 2(13). The convergence of energy by succesive inclusion of these states is shown in Table I. By combining the cluster arrangements the energy converges even with the use of $l_1=l_2=0$ partial waves only. By expanding the wave function in one particular Jacobi system up to $l_1=l_2\leq 4$, however, one still misses

reaching the full convergence. By using a properly antisymmetrized wave function of three indistinguishable nucleons, one gets the same energy as in the case of the combination of the arrangements (12)3, 1(23), and 2(13). The dimension of the basis in the calculations was around 20.

In the case of the four-nucleon system ($L=0$), the $(2N)+(2N)$ and $(3N)+N$ arrangements were used and partial waves satisfying the conditions $(-1)^{l_1+l_2+l_3}=1$, $l_1+l_2+l_3\leq 2$ were coupled. The results are compared in Table I. It is impressive that the solutions by the SVM agree very well with those of other methods. One can see in Table I that if we use only one arrangement and truncate the partial waves to $l_1=l_2=l_3=0$, then a considerable amount of the binding energy is missing. Table I also shows that the convergence of the energy with including higher partial waves in a given arrangement is rather slow. The calculation of matrix elements with higher partial waves, at the same time, especially for complex systems, is rather time consuming and would make the calculation unfeasible. By combining, however, the two arrangements, $(2N)+(2N)$ and $(3N)+N$, including only $l_1=l_2=l_3=0$ partial waves, the energy becomes -30.42 MeV and this value changes less than 0.001 MeV by including higher partial waves.

The optimal choice of the variational basis is a very difficult task because of either of the following reasons: (1) the optimization of nonlinear parameters is tedious or (2) if all parameters are linear, then the size of the basis becomes extremely large. We have tried to optimize the basis by using Powell's method [23], but we failed to optimize more than 60 nonlinear parameters at the same time because the optimization became extremely slow and was often trapped in poor local extrema. This optimization worked very nicely in a three-body problem but the 60 nonlinear parameters were not enough to find the best energy in four-body case. The use of some more advanced optimization strategy could partly solve this problem but the high numerical cost of the evalution of the matrix elements can make such calculations too time consuming. In the second alternative, one chooses the size parameters of the basis as a geometric progression [20]. Thus the number of nonlinear parameters is reduced to the two parameters of the geometric progression that can more easily be optimized or selected by physical intuition. One serious problem here is that the dimension of the basis becomes very large even for a four-body system. By assuming that k size parameters are sufficient to expand the function of the relative motion (k is usually about 6–10), the dimension of the basis for a four-body system is k^3 times the number of different angular momentum channels of relative motions. The SVM lies somewhere between these two alternatives. The nonlinear parameters are not fully optimized, but the dimension is kept low by selecting new elements which are sufficiently good with respect to the previously selected ones.

III. RESULTS

A. Input parameters

We approximate the internal states of α, t, and h by $0s$ harmonic-oscillator Slater determinant wave functions of a common width parameter. The width parameter $\beta=m\omega/\hbar$ is adjusted to get nearly correct values for the sum of the radii of the free α plus t and α plus h clusters and to minimize their energies ($\beta=0.52$ fm^{-2}). The results are not too sensitive to the choice of the size parameter within a reasonable limit, as we will discuss later.

We used a Minnesota effective nucleon-nucleon interaction [24], which is a sum of central, Coulomb, and spin-orbit potentials of Gaussian form. The strength of the spin-orbit force was set to give the correct spacing between the $3/2^-$ and $1/2^-$ states of the ^{7}Li and ^{7}Be subsystems. The u parameter of the central part was set to get overall agreement between the experimental and model energies of the states of ^{7}Be, ^{8}B, ^{7}Li, and ^{8}Li ($u=1.00$). This force, by setting the u parameter to the five- and seven-nucleon systems, was succesfully used earlier to describe the ^{5}Li, ^{5}He, ^{7}Li, and ^{7}Be nuclei in various models [6,11]. By fixing the u and β parameters as described above, the model contains no free parameter. We note that we tried different choices of the size parameter β and changed u accordingly, but the separation energies and sizes of the two-, three-, and four-body systems remained nearly the same. We accepted the present value as it minimizes the sum of the energies of the free clusters.

For the calculation of the bound $3/2^-$ and $1/2^-$ states of ^{7}Be and ^{7}Li the $l=1$ partial wave and 7 size parameters were used. The experimental and calculated separation energies of the $3/2^-$ ground states of ^{7}Be and ^{7}Li will be compared later (see Fig. 2). The level spacings between the $3/2^-$ ground states and the $1/2^-$ excited states of these nuclei are correct as the strength of the spin-orbit force was adjusted to reproduce it: $E_{1/2^-}-E_{3/2^-}=0.50$ MeV in the model (0.48 MeV experimentally) for ^{7}Li and $E_{1/2^-}-E_{3/2^-}=0.48$ MeV in the model (0.43 MeV experimentally) for ^{7}Be.

B. Angular momentum channels

The model space of the 2^+ ground state of the ^{8}Li and ^{8}B nuclei was constructed by using all arrangements and angular momentum configurations that can be physically relevant. To build up the intuitively most important configuration, we added one nucleon with $l_2=1$ to the $^7\text{Li}=\alpha+t$ and $^7\text{Be}=\alpha+h$ two-cluster systems with $l_1=1$ and coupled the relevant angular momenta to form the 2^+ configuration. The $^5\text{He}=\alpha+n$ plus t and the $^5\text{Li}=\alpha+p$ plus h partitions,

TABLE II. Cluster decomposition of ^{8}Li and ^{8}B. The arrangements in the first column are those of ^{8}Li. The corresponding mirror arrangements are not shown.

	Channel				Amount of clustering	
Arrangement	l_1	l_2	L	S	^{8}Li	^{8}B
$(\alpha t)n$	1	1	1	1	0.95	0.96
	1	1	2	0	0.01	0.01
	1	1	2	1	0.02	0.01
$(\alpha n)t$	1	1	1	1	0.95	0.95
	1	1	2	0	0.02	0.01
	1	1	2	1	0.01	0.01
$(tn)\alpha$	1	1	1	1	0.94	0.94
	1	1	2	0	0.01	0.01
	1	1	2	1	0.01	0.01

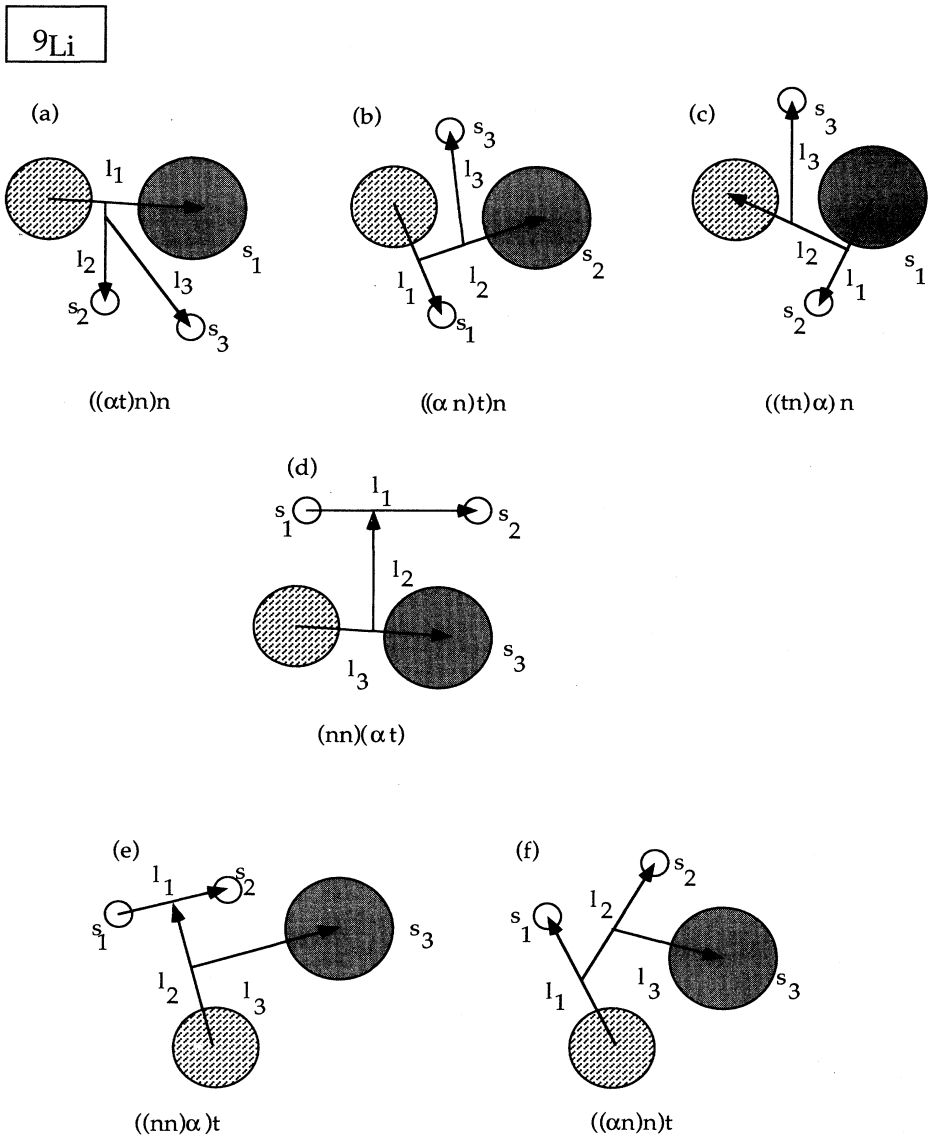

FIG. 1. Different arrangements used in the calculation for ^{9}Li. The small circles are neutrons, the medium-size circle is the alpha particle, and the largest circle is the triton. The orbital angular momenta for the relative motion between the clusters connected by solid line are denoted by l_i. The spin of the clusters is $s_i = 1/2$; the spin of the alpha particle is zero and it is omitted.

which lie 0.89 MeV and 1.97 MeV above the three-body threshold, are also included with appropriate angular momentum labels. Finally we included the higher-lying $\alpha(tn)$ and $\alpha(hp)$ arrangements. As the even partial waves are not favorable for the $\alpha+n$, $t+n$, and $\alpha+t$ (and of the corresponding mirror) relative motions, the lowest physically important partial wave set to form a positive parity state is $l_1=l_2=1$. The higher partial waves ($l_1=1, l_2=3$ and $l_1=3, l_2=1$) were found to give no significant contribution to the energy and to the wave function. The spins of the clusters were coupled to $S=0,1$. The list of the cluster arrangements and angular momentum channels found important and used in the calculation is given in Table II.

To describe ^{9}Li in the $\alpha+t+n+n$ four-body model all Jacobi arrangements and angular momentum sets are included that are expected to be important: The $((\alpha t)n)n$ configuration [see Fig. 1(a)] is best suited to describe a ^{7}Li$+n+n$ "shell-model-like" configuration. The arrangements $((\alpha n)t)n$ [Fig. 1(b)] and $((tn)\alpha)n$ [Fig. 1(c)] emphasize the correlation between the α particle and a neutron and the triton and a neutron, respectively. The arrangement $(nn)(\alpha t)$ [Fig. 1(d)] prefers a ^{7}Li plus a dineutron cluster. The arrangements in Figs. 1(e) and 1(f) correspond to ^{6}He$+t$-type fragmentation containing the $\alpha(nn)$ and $(\alpha n)n$ subsystems that are found to be important to describe the ^{6}He nucleus [1,3]. The first three arrangements [Figs. 1(a), 1(b), and 1(c)] can also be viewed as ^{8}Li$+n$-type configurations because they include the same three-body Jacobi coordinate systems $(\alpha t)n$ [Fig. 1(a)], $(\alpha n)t$ [Fig. 1(b)], and $(tn)\alpha$ [Fig. 1(c)] as those used in the description of ^{8}Li.

This four-cluster model with different arrangements can be related to the multiconfiguration multicluster model [6]. In the multiconfiguration multicluster model one divides the nucleus into different two-cluster systems allowing for excited states of the clusters as well, and combines those configurations to form the wave function. In this framework our model can be considered a combination of ^{8}Li$+n$,

TABLE III. Energies, matter radii, and quadrupole moments of ^{8}Li and ^{8}B in different subspaces. If for a given arrangement the angular momenta $(l_1 l_2)LS$ are not specified, then all sets listed in Table II are included. The arrangements belong to ^{8}Li. The corresponding mirror arrangements are not shown. The experimental energies are -4.50 MeV for ^{8}Li and -1.73 MeV for ^{8}B. The configurations of ^{8}B marked by an asterisk are unbound with respect to the ^{7}Be$+p$ threshold. The energy of ^{7}Be relative to the $\alpha+h$ threshold is -1.60 MeV.

Subspace configuration	E (MeV)		r (fm)		Q (e fm^2)	
	^{8}Li	^{8}B	^{8}Li	^{8}B	^{8}Li	^{8}B
$(\alpha t)n$: (11)11	-3.90	-1.60*	2.43	--	2.01	--
$(\alpha n)t$: (11)11	-3.64	-1.60*	2.53	--	1.59	--
$(tn)\alpha$: (11)11	-3.37	-1.60*	2.44	--	1.50	--
$(\alpha t)n$: (11)11, (11)21, (11)20	-4.03	-1.60*	2.42	--	2.11	--
$(\alpha t)n$	-4.09	-1.60*	2.41	--	2.14	--
$(\alpha n)t$	-3.80	-1.60*	2.49	--	2.18	--
$(tn)\alpha$	-3.53	-1.60*	2.42	--	1.87	--
$(\alpha t)n+(\alpha n)t$	-4.24	-1.73	2.45	2.56	2.19	6.71
$(\alpha t)n+(tn)\alpha$	-4.22	-1.69	2.42	2.50	2.24	6.48
$(\alpha n)t+(tn)\alpha$	-4.06	-1.60*	2.45	--	2.14	--
$(\alpha t)n+(\alpha n)t+(tn)\alpha$: (11)11	-4.09	-1.66	2.44	2.62	2.17	5.80
full model	-4.31	-1.78	2.44	2.56	2.23	6.65

^{7}Li$+(nn)$, and ^{6}He$+t$ two-cluster systems including excited states of the constituents.

To form the $3/2^-$ ground state of ^{9}Li we assume the total orbital angular momentum to be $L=1$ and couple the spins of the clusters to $S=1/2$. We restrict ourselves to the lowest possible partial wave sets: $l_1=1, l_2=0, l_3=0$; $l_1=0, l_2=1, l_3=0$; $l_1=0, l_2=0, l_3=1$; and $l_1=l_2=l_3=1$. The partial waves (see Fig. 1) are coupled as $((l_1 l_2)l_{12} l_3)L$ and the spins of the clusters $s_1=s_2=s_3=1/2$ (see Fig.1) combined as $((s_1 s_2)s_{12} s_3)S$ to form the total spin S. (The spin of the α particle is zero and we omitted it to simplify the notation.) The intermediate quantun numbers l_{12} and s_{12} are chosen to be $l_{12}=0,1$ and $s_{12}=0,1$. The number of possible configurations is reduced by excluding the unfavorable even partial waves from the $\alpha+t$, $\alpha+n$, and $t+n$ relative motions and the two-neutron configurations in singlet-odd or triplet-even relative states. The model space defined by combining the cluster arrangements with these angular momentum labels will be referred as model space A.

C. Cluster decompositions

To explore the relevance of the different cluster arrangements and the angular momentum decompositions we performed several test calculations restricting the model space by omitting configurations. These pilot calculations reveal the relative importance of the different channels and check the completeness of the model space. In the first example, we included only the presumably most important configuration: the $(\alpha t)n$ arrangement with $(l_1 l_2)LS=(11)11$ for ^{8}Li (see Table III). The binding energy of ^{8}Li was 0.4 MeV smaller than in the full calculation and the quadrupole moment also decreased by 10%. Different Jacobi coordinate systems with the same $(l_1 l_2)LS=(11)11$ angular momentum channel give different energies, showing the different natures of the cluster arrangements. By including other angular momentum components in the $(\alpha t)n$ arrangement, the energy decreases but, as we mentioned before, the convergence is slow. We also calculated the energy in different cluster arrangements using all angular momentum sets that are listed in Table II. The $(\alpha t)n$ arrangement gives the lowest energy for ^{8}Li as one may expect, but none of the arrangements gives a bound state for ^{8}B with respect to the ^{7}Be$+p$ threshold. We then combined two arrangements in all possible ways to see whether any of the three arrangements can be omitted. The results suggest the relative importance of the $(\alpha t)n$ and $(\alpha n)t$ configurations, but no arrangement seems to be redundant. The full calculation was repeated several times and was terminated when we had convergence for not only the energy but also the calculated physical quantities. The dimension of the basis was about 80. To check the completeness of the model space we included some other partial waves such as $(l_1 l_2)=(33),(13),(31)$, as well. The energy changed less than 0.01 MeV so that the model space is nearly complete. In the case of ^{8}B, due to its small binding energy, one should be careful in building up the wave function.

The wave function in this nonorthogonal basis can be characterized by the "amount of clustering" [25]. The amount of clustering is defined as the weight of the component of the wave function that lies in the subspace of the model space associated with that particular clusterization. Each subspace bears an arrangement label μ and a set of angular momentum labels. Since the subspaces are not orthogonal, the sum of the amount of clustering over the subspaces is not necessarily unity. These weights for the various channels are listed in Table II. One finds that each arrangement with $(l_1 l_2)LS=(11)11$ angular momentum label has large and almost equal weight, but, as one learns from Table III, if the other angular momentum components are neglected, the binding energy decreases considerably. The weights of the components of the wave function with different angular momenta $(L,S)=(1,1)$, $(2,0)$, and $(2,1)$ are 96.0%, 1.6%, and 2.4% in ^{8}Li and 96.5%, 1.6%, and 1.9% in ^{8}B.

TABLE IV. Cluster decomposition of ^{9}Li and ^{9}C. The arrangements in the first column are those of ^{9}Li. The corresponding mirror arrangements are not shown. See also Fig. 1. $L=1$, $S=1/2$, $J=3/2$.

Arrangement	Channel l_1	l_2	l_{12}	l_3	s_{12}	Amount of clustering ^{9}Li	^{9}C
$((\alpha t)n)n$	1	1	1	1	1	0.89	0.84
	1	0	1	0	0	0.19	0.20
	1	0	1	0	1	0.09	0.12
$((\alpha n)t)n$	1	1	1	1	1	0.87	0.86
	1	0	1	0	0	0.11	0.11
	1	0	1	0	1	0.07	0.06
$((tn)\alpha)n$	1	1	1	1	1	0.80	0.82
	1	0	1	0	0	0.13	0.14
$(nn)(\alpha t)$	0	0	0	1	0	0.40	0.44
$((nn)\alpha)t$	0	0	0	1	0	0.34	0.22
	0	1	0	1	0	0.21	0.13
$((\alpha n)n)t$	1	0	1	0	0	0.43	0.29
	1	1	0	1	0	0.23	0.17

To find the most important configurations of the four-cluster system, we first carried out a calculation in model space A. Test calculations show that this model space is close to a complete set and the inclusion of a few higher partial waves does not change the energy and the radius of the four-body systems. The physical quantities calculated in model space A will be discussed later. (See Tables V and VI, below.) This model space, however, is quite extensive. The wave function in this model space is a combination of dozens of different components (cluster arrangements with various angular momentum labels), and many of these components have only a small weight in the total wave function. To understand the structure of the wave functions and the physical significance of the different components, it is worthwhile to define a model space by selecting only a few dominant configurations. To this end we have calculated the weights (amounts of clustering) of the components of the selected wave function in model space A and defined a model space (model space B) for ^{9}Li and ^{9}C by excluding the angular momentum channels with weights less than 0.03. This model space B consists of the most important configurations (see Table IV). [A similar reduction of the model space can be achieved by using a larger value for ε of the acceptance criteria in Eq. (5).] The calculation in model space B shows that the energy increases by 0.31 MeV in the case of ^{9}Li and by 0.13 MeV in the case of ^{9}C. The calculated physical quantities (magnetic and quadrupole moments, proton, and neutron radii), at the same time, remain essentially the same (see Table V). By accepting this energy loss as the price for a simpler model space, one may use model space B to investigate the role of the different cluster arrangements and to show the relative importance of the most important configurations. This model space may also be a starting point to build up the model space of the more challenging $\alpha+t+n+n+n+n$-type six-cluster calculation for ^{11}Li.

The effect of the omission of cluster arrangements is investigated in Table V. The four-body separation energy of ^{9}Li is 0.3–1.5 MeV smaller in a single cluster arrangement calculation than in the full calculation including all configurations listed in Table IV. The matter radius and quadrupole moment are somewhat more diverse in different arrangements than they were in the case of ^{8}Li, due probably to the differences in separation energies. The basis size of the calculation in model space B is about 150.

In the case of the four-cluster systems the wave function is more complex than in the case of ^{8}Li and ^{8}B (see Table II and Table IV), and the interplay between the different components seems to be important. We conclude that the wave functions of these three- and four-cluster systems are combinations of various different components and, although some of these components have small weights, they contribute to the energy and to the physical quantities considerably. A neglect of these components requires due care especially in the case of light exotic nuclei with extended density distribution. It is worthwhile to emphasize here that repeating the calculation starting from different random points leads to the same weights up to the digits shown in the tables.

TABLE V. Energies, matter radii, and quadrupole moments of ^{9}Li and ^{9}C in different subspaces. All sets of the angular momenta that belong to a given arrangement in Table IV are included for the first six configurations. The model space A is an extensive model space defined in Sec. III B. The model space B is the combination of those configurations that are listed in Table IV. The arrangements belong to ^{9}Li and the corresponding mirror channels are not shown. The experimental energies are -8.56 MeV for ^{9}Li and -3.02 MeV for ^{9}C.

Subspace configuration	E (MeV) ^{9}Li	^{9}C	r (fm) ^{9}Li	^{9}C	Q (e fm^2) ^{9}Li	^{9}C
$((\alpha t)n)n$	-7.18	-1.96	2.43	2.47	-2.55	-5.16
$(\alpha t)(nn)$	-6.98	-1.90	2.38	2.47	-2.60	-5.22
$((nn)\alpha)t$	-6.01	-1.77	2.37	2.58	-2.30	-5.41
$(\alpha(tn))n$	-7.05	-1.98	2.40	2.53	-2.80	-5.29
$((\alpha t)n)n+(\alpha(tn))n+((\alpha n)t)n$	-7.24	-2.04	2.40	2.49	-2.72	-5.12
$((nn)\alpha)t+((\alpha n)n)t$	-6.35	-1.85	2.35	2.56	-2.39	-5.44
model space B	-7.74	-2.49	2.39	2.50	-2.69	-5.09
model space A	-8.05	-2.62	2.39	2.50	-2.74	-5.04

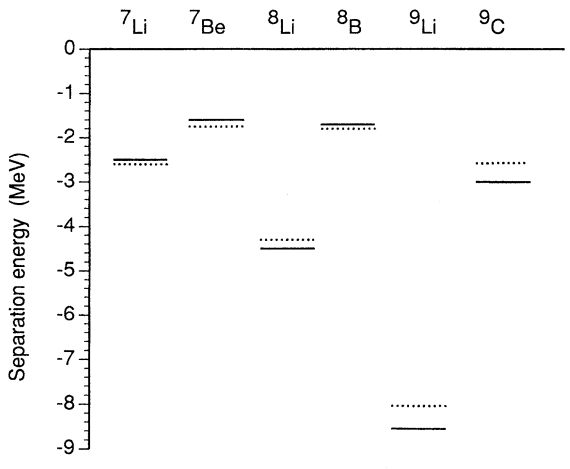

FIG. 2. Experimental (solid line) and calculated (dotted line) energies of the two-, three-, and four-body systems.

D. Comparison with experiment

The calculated and experimental energies of the ground states are compared in Fig. 2. The overall agreement is reasonably good. The ^{7}Li, ^{7}Be, and ^{8}B nuclei are slightly overbound, while the ^{8}Li, ^{9}Li, and ^{9}C nuclei are somewhat underbound. One cannot expect to improve the model energies further by using the same effective nucleon-nucleon interaction for all of these nuclei. The calculated physical quantities, in test runs, did not show strong sensitivity to small changes in the model energy. That is, if we tune the force parameter u for any of the systems separately, so as to take the model energy closer to the experimental value, the results do not change substantially. Such a tuning of the parameters, however, would make the calculated quantities of different nuclei incomparable.

The proton, the neutron, and the matter radii, assuming pointlike nucleons, are included in Table VI. The only information about the size of the unstable systems comes from the measurement of their interaction cross sections on different targets. The proton, neutron, and matter radii are then determined by assuming some simple (usually Gaussian or harmonic-oscillator) density distributions in Glauber-type reaction models and fitting the interaction cross section data [26]. These model-dependent empirical data are listed in the "experimental" line of the Table VI. The interaction cross section of ^{9}C on carbon target at 800 MeV/nucleon has recently been measured, and found to be slightly larger than that of ^{9}Li. The empirical radii of ^{9}C are, therefore, supposed to be close to the mirror values, but the empirical radii of ^{9}C have not been determined yet.

The model and the empirical data are in good agreement for the Li isotopes, but the agreement for the proton-rich side is not so good. The interaction cross sections of the mirror pairs were found nearly the same experimentally. The corresponding empirical radii therefore are almost equal for mirror pairs. The model, however, tends to give larger radii for the proton-rich side. This seems to be reasonable because, due to the repulsive Coulomb interaction, the separation energies (see Fig. 2) of ^{7}Be, ^{8}B, ^{9}C are much smaller than those of the respective mirror nuclei (the difference between the separation energies of ^{8}Li and ^{8}B is 2.8 MeV and that of ^{9}Li and ^{9}C is 5.5 MeV), and therefore they are less tight systems. The larger radii on the proton-rich side can be attributed to the difference in the density distributions at large distances, as shown later.

The difference of proton and neutron radii, the skin "thickness," is less than 0.5 fm in all cases. The thickest skin is found in the case of ^{8}B (0.49 fm) and ^{9}C (0.48 fm). These differences seem to be reasonable consequences of the large proton excess. On the neutron-rich side, the thickness of skin of ^{8}Li and ^{9}Li is about 0.4 fm.

The experimental information on the magnetic and quadrupole moments is also available for some of these nuclei. These moments may serve as probes of the spatial extension and angular momentum content of the model wave function. No effective charge was employed. The calculated magnetic and quadrupole moments also agree well with the available experimental data. The only noticeable disagreement occurs in the case of the magnetic moment of ^{8}Li and ^{8}B. Most likely this is a consequence of the fact that we approximated the internal states of h and t by single Slater determinants. In this simple description of the three-nucleon clusters, the two like nucleons have opposite spins and the contribution of the spins to the magnetic moment comes from the third nucleon. The magnetic moments of t and h in our model are, therefore, taken equal to those of the proton and neutron, respectively. If, instead, the observed values of the magnetic moments were used, the discrepancies in the ^{8}Li and ^{8}B magnetic moments would be significantly reduced.

The quadrupole moments of ^{7}Be and ^{9}C have not yet been determined experimentally. The model predictions for the quadrupole moment of ^{7}Be is -6.11 e fm^2, and that of ^{9}C is -5.04 e fm^2.

E. Density distributions

The proton and the neutron density distributions, defined by

$$\rho(\mathbf{r})=\left\langle \Psi \left| \sum_{i=1}^{A} \delta(\mathbf{r}_i-\mathbf{R}_{\text{c.m.}}-\mathbf{r})P_i \right| \Psi \right\rangle = \sum_l \rho_l(r)Y_{l0}(\hat{\mathbf{r}}) \tag{7}$$

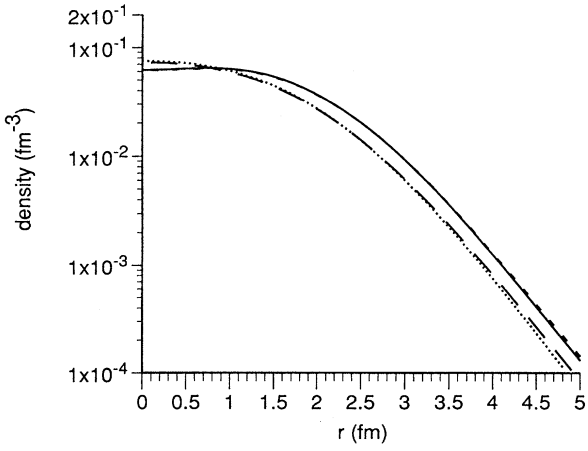

FIG. 3. Proton density distribution of ^{7}Be (short dashed line), ^{7}Li (dotted line), and neutron density distribution of ^{7}Be (long dashed line), ^{7}Li (solid line).

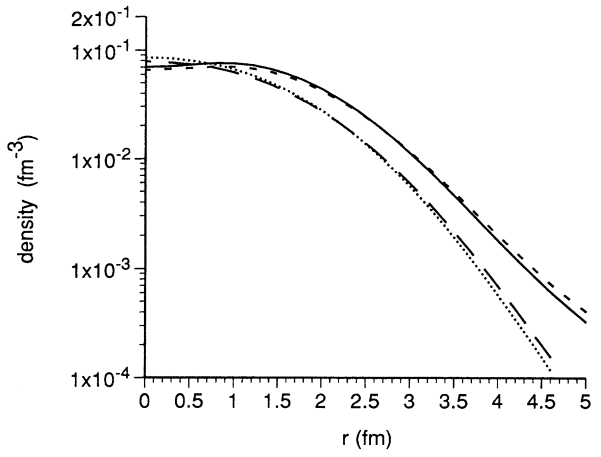

FIG. 4. Proton density distribution of ^{8}B (short dashed line), ^{8}Li (dotted line), and neutron density distribution of ^{8}B (long dashed line), ^{8}Li (solid line).

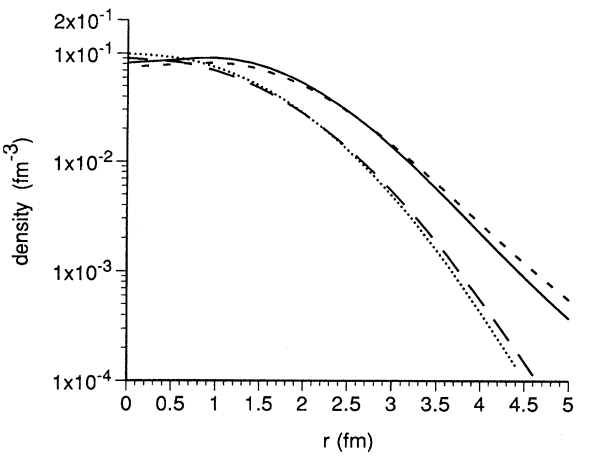

FIG. 5. Proton density distribution of ^{9}C (short dashed line), ^{9}Li (dotted line), and neutron density distribution of ^{9}C (long dashed line), ^{9}Li (solid line).

(where P_i projects out the protons or neutrons), are also determined. The density distributions $\rho_0(r)/\sqrt{4\pi}$, belonging to $l=0$ partial wave are shown in Figs. 3–5. The nucleon distributions in the ^{7}Li and ^{7}B nuclei are rather alike (Fig. 3). The tail part of the proton distribution of ^{8}B is significantly larger than that of ^{8}Li (Fig. 4), causing considerable difference in the radii (see Table VI). The difference between the proton and neutron density distributions of ^{9}C is even larger than that of ^{8}B (Fig. 5), but this is natural as it has one more proton. The difference between the proton and neutron radii, at the same time, is nearly the same.

The density distributions of ^{8}B (Fig. 6) and of ^{9}Li (Fig. 7) of our model are compared to those of the pure harmonic-oscillator shell model. In the pure harmonic-oscillator shell model limit of our model the wave functions of relative motions are approximated by harmonic-oscillator functions. In this limiting case the microscopic multicluster model reduces to an LS coupled harmonic-oscillator shell model. The size parameter of the harmonic-oscillator model is chosen to fit the empirical radii. As one can expect, the density distribution of the harmonic-oscillator shell model decreases very quickly at the nuclear surface. The density in the multicluster model, on the contrary, has a long, slowly decreasing tail. This tail part gives non-negligible contributions to the radii and quadrupole moments even at about 10 fm $[r^2\times r^2\rho(r)=10^2\ \text{fm}^2\times 10^2\ \text{fm}^2\times 10^{-6}\ \text{fm}^{-3}]$, and certainly

TABLE VI. Proton, neutron, and matter radii, and quadrupole and magnetic moments. The empirical radii are from Ref. [26].

	μ (μ_N)	Q (e fm^2)	r_m (fm)	r_p (fm)	r_n (fm)
^{7}Be ($3/2^-$) expt.	– – – –	– – – –	2.31	2.36	2.25
^{7}Be ($3/2^-$) model	−1.27	−6.11	2.36	2.41	2.31
^{7}Li ($3/2^-$) expt.	3.26	−4.00±0.06 [a]	2.33	2.27	2.38
^{7}Li ($3/2^-$) model	3.15	−3.65	2.33	2.27	2.38
^{8}B (2^+) expt.	1.04	6.83±0.21 [b]	2.38	2.45	2.27
^{8}B (2^+) model	1.42	6.65	2.56	2.73	2.24
^{8}Li (2^+) expt.	1.65	3.27±0.06 [b], 3.11±0.05 [c]	2.37	2.26	2.44
^{8}Li (2^+) model	1.17	2.23	2.44	2.18	2.58
^{9}C ($3/2^-$) expt.	|1.39| [d]	– – – –	– – – –	– – – –	– – – –
^{9}C ($3/2^-$) model	−1.50	−5.04	2.50	2.64	2.16
^{9}Li ($3/2^-$) expt.	3.44	−2.74 [c]	2.32	2.18	2.39
^{9}Li ($3/2^-$) model	3.43	−2.74	2.39	2.10	2.52

[a]Quadrupole moments from Ref. [27], magnetic moments from Ref. [30].
[b]Quadrupole moments from Ref. [28], magnetic moments from Ref. [30].
[c]Quadrupole moments from Ref. [29], magnetic moments from Ref. [30].
[d]Magnetic moments from Ref. [5].

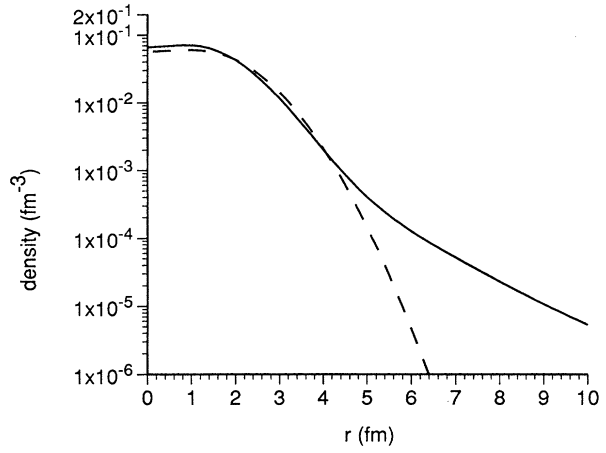

FIG. 6. Proton density of ^{8}B in the present model (solid line) and in a pure harmonic-oscillator shell model (dashed line).

plays a very important role in astrophysical processes and reaction mechanisms. The long tail of ^{9}Li is also expected to give some contribution to the binding mechanism of ^{11}Li: It leads to a ^{9}Li-n potential of longer range, and makes the effects of the Pauli principle stronger than that deduced in a harmonic-oscillator approximation. A full understanding of the structure of ^{11}Li will thus call for this microscopic structure of ^{9}Li even in the ^{9}Li$+n+n$ three-body approach.

Two other quantities that can be used to characterize the spatial distribution of the nucleons are the one- and two-nucleon removal spectroscopic amplitudes. The one-proton removal amplitude of ^{8}B is defined as

$$g^p(\mathbf{r})=\langle\Psi(^7\mathrm{Be})\,\delta(\mathbf{r}-\boldsymbol{\rho})|\Psi(^8\mathrm{B})\rangle=\sum_{jl} g^p_{jl}(r)Y_l(\hat{\mathbf{r}}), \quad (8)$$

with

$$g^p_{jl}(r)=\int d\hat{\mathbf{r}}\langle[[\Psi_S(^7\mathrm{Be})\xi^p_s]_j Y_l(\hat{\mathbf{r}})]_{JM}\,\delta(\mathbf{r}-\boldsymbol{\rho})|\Psi_{JM}(^8\mathrm{B})\rangle, \quad (9)$$

where $\Psi_{JM}(A)$ ($A=^7$Be,^{7}Li,^{8}B,^{8}Li) is the model wave function of the corresponding nuclei of spin J, ξ^p_s is the spin function of the proton, and $\mathbf{r}$ is the position of the nucleon with respect to the center of mass of the "core." Similarly, the two-proton removal amplitudes of ^{9}C are

$$g^{pp}(\mathbf{r},\mathbf{R})=\langle\Psi(^7\mathrm{Be})\,\delta(\mathbf{r}-\boldsymbol{\rho}_1)\,\delta(\mathbf{R}-\boldsymbol{\rho}_2)|\Psi(^9\mathrm{C})\rangle=\sum_{sjl_1l_2L} g^{pp}_{sjl_1l_2L}(r,R)[Y_{l_1}(\hat{\mathbf{r}})Y_{l_2}(\hat{\mathbf{R}})]_L, \quad (10)$$

with

$$g^{pp}_{sjl_1l_2L}(r,R)=\int d\hat{\mathbf{r}}d\hat{\mathbf{R}}\langle[[\Psi_S(^7\mathrm{Be})\xi^{pp}_s]_j[Y_{l_1}(\hat{\mathbf{r}})Y_{l_2}(\hat{\mathbf{R}})]_L]_{JM}\,\delta(\mathbf{r}-\boldsymbol{\rho}_1)\,\delta(\mathbf{R}-\boldsymbol{\rho}_2)|\Psi_{JM}(^9\mathrm{C})\rangle, \quad (11)$$

where $\mathbf{r}$ is the distance between the two nucleons and $\mathbf{R}$ is the distance between the center of mass of the two nucleons and that of the core and ξ^{pp}_s is the spin function of the two protons. The corresponding mirror quantities can be defined in the same way.

The one-proton removal amplitude of ^{8}B and the one-neutron removal amplitude of ^{8}Li are compared in Fig. 8. The amplitudes belong to the first nonvanishing partial wave ($l=1,j=1$). The shapes of the amplitudes are rather similar; both amplitudes have maxima at about 2.5 fm (the last nucleon is on the surface of ^{7}Be and ^{7}Li). The tail part of the proton removal amplitude is, however, larger and more slowly decreasing as a consequence of the tiny proton separation energy (0.14 MeV) of ^{8}B. The norms of these amplitudes, the one-nucleon spectroscopic factors, are nearly equal (both are about 1.22).

The largest components of the two-nucleon removal amplitudes are drawn in Fig. 9(a) and Fig. 9(b). These components belong to zero partial waves ($l_1=l_2=L=0,j=3/2$) and the two like nucleons are in a spin singlet state ($s=0$). The two-proton and two-neutron distributions are again quite similar. There is a broader maximum at $r=2$ fm, $R=2.8$ fm ($r=1.8$ fm, $R=2.5$ fm) in the two-proton (two-neutron) removal amplitude. This peak roughly corresponds to a picture where the two nucleons are on the surface of the "core." The distance between the two nucleons is smaller than the average distance between the proton and neutron in the deuteron (which is about 4 fm), but they do not form so compact a dineutron configuration that we found in the case of ^{6}He and ^{8}He [3]. The other maximum is at $r=4.7$ fm, $R=0.8$ fm for ^{9}C and at $r=4.3$ fm, $R=1.0$ fm in the case of ^{9}Li. This can be visualized as two nucleons sitting at the opposite sides of the core. Because of the Coulomb repulsion, the ^{9}C is somewhat less tight.

IV. SUMMARY AND DISCUSSION

By using the microscopic multicluster model combined with the stochastic variational method we studied the ^{7}Be-^{7}Li, ^{8}B-^{8}Li, and ^{9}C-^{9}Li nuclei. The nuclei are described in two-, three-, and four-cluster models comprising α, t, h, and single-nucleon clusters. The same effective nucleon-nucleon interaction and model space are used for all systems. The stochastic variational method worked very nicely in these multicluster systems. The separation energies are reasonably reproduced. The calculated point matter radii are close to the "empirical" values for the Li isotopes, but for the ^{8}B and ^{9}C nuclei exceed them (see Table VI). The

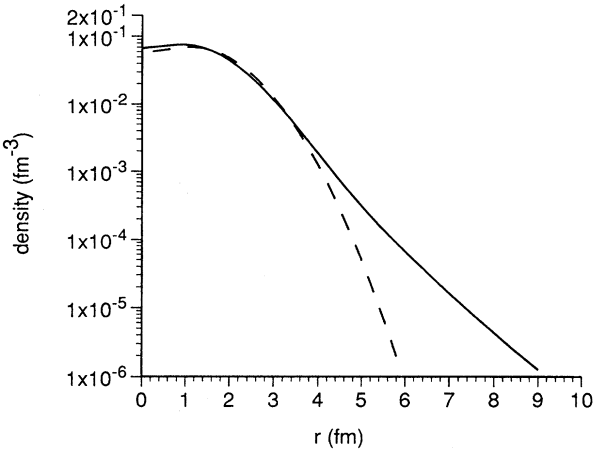

FIG. 7. Neutron density of ^{9}Li in the present model (solid line) and in a pure harmonic-oscillator shell model (dashed line).

most striking disagreement appears in the case of ^{8}B. Other theoretical models [9,14,13] also tend to overestimate the radius (3.03 fm in Ref. [9], 2.74 fm in Ref. [14], 2.88 fm in Ref. [13]), while their predictions for the quadrupole moment are nearly correct. At the same time, the calculated thickness of the proton (neutron) skin of ^{8}B (^{8}Li) is nearly the same in cluster models [0.42 fm (0.35 fm) in Ref. [13], 0.49 fm (0.39 fm) in Ref. [14], and 0.49 fm (0.4 fm) in the present model].

The point-matter root-mean-square radii of ^{9}Li and ^{9}C are smaller than those of ^{8}Li and ^{8}B. This can be understood in a simple shell model picture as a consequence of the closing of the $p_{3/2}$ neutron (proton) orbits of ^{9}Li (^{9}C). The empirical radii were extracted—in a model-dependent analysis—using the measured interaction cross section data. To relate the model and the experimental results more directly, one has to calculate the experimentally observed interaction cross sections, rather than the empirically determined radii. This can be achieved by the help of the Glauber theory [31] using the densities and wave functions determined in the model [32]. Such a calculation is planned in the near future.

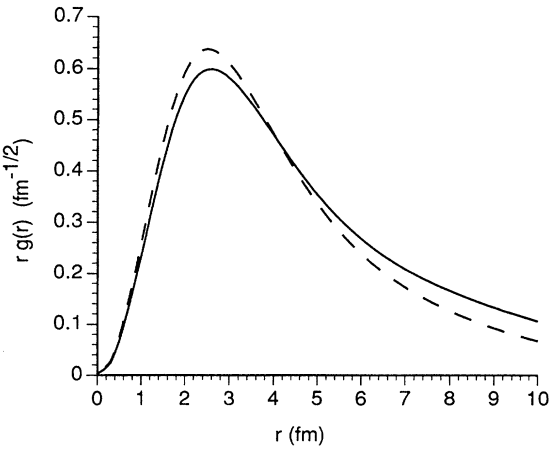

FIG. 8. One-proton (solid line) and one-neutron (dashed line) removal spectroscopic amplitudes of ^{8}B and ^{8}Li, respectively.

The microscopic multicluster model predicts that the neutron skin thickness is about 0.4 fm in ^{8}Li and ^{9}Li, while the proton skin thickness is 0.5 fm in ^{8}B and ^{9}C. Comparing to the neutron skin thickness of 0.8 fm found in ^{6}He and ^{8}He [3], we conclude that these nuclei do not show pronounced halo structure.

The calculated magnetic and quadrupole moments, except the magnetic moments of ^{8}Li and ^{8}B, are in reasonable agreement with the available data. An accurate description of the tail parts of the wave functions of ^{8}B and ^{9}C is needed to calculate their quadrupole moments. The model prediction is -6.11 e fm^2 for the quadrupole moment of ^{7}Be and -5.04 e fm^2 for that of ^{9}C. These data will be available experimentally in the near future [5].

Although the neutron halo in ^{9}Li is not pronounced, the falloff of the neutron density distribution is much slower than that of the shell model prediction. We pointed out that this effect should be taken into account for a complete description of ^{11}Li.

ACKNOWLEDGMENTS

We would like to thank Dr. T. Kobayashi, Dr. A. Ozawa, and Dr. H. Kitagawa for useful discussions. K.V. gratefully

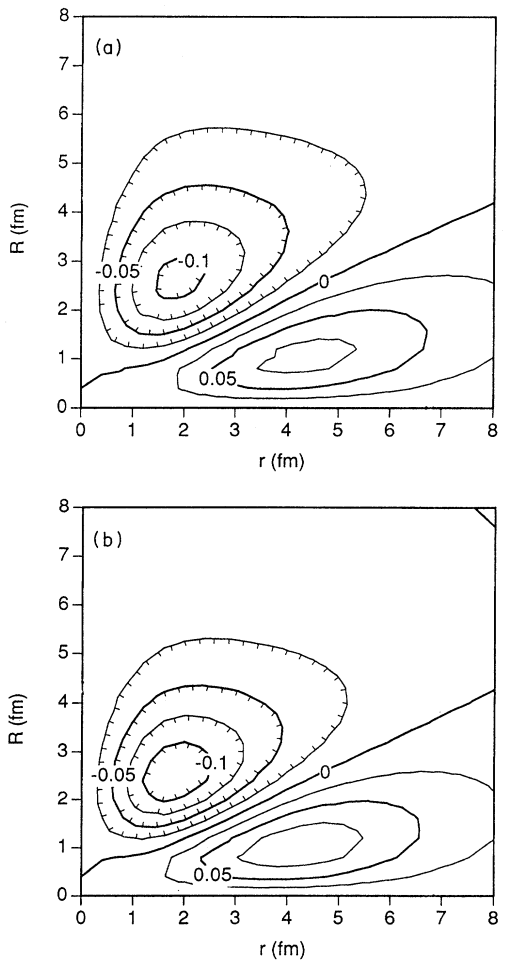

FIG. 9. Two-proton (a) and two-neutron (b) removal spectroscopic amplitudes of ^{9}C and ^{9}Li, respectively.

acknowledges the support from the Science and Technology Agency of Japan and the hospitality of the LINAC laboratory of the RIKEN. This work was supported by OTKA Grants No. 3010 and No. F4348 (Hungary) and by a Grant-in-Aid for Scientific Research (No. 05243102 and No. 0664038) of the Ministry of Education, Science and Culture (Japan).

APPENDIX A

We give the detailed form of the trial function of ^{8}Li in the $(\alpha t)n$ arrangement as an example. The Jacobi coordinates of the $(\alpha t)n$ arrangement are defined as

$$\boldsymbol{\rho}_1^{(\alpha t)n}=\mathbf{r}_t-\mathbf{r}_\alpha,$$

$$\boldsymbol{\rho}_2^{(\alpha t)n}=\mathbf{r}_n-\frac{4\mathbf{r}_\alpha+3\mathbf{r}_t}{7},$$

$$\mathbf{R}_{\alpha tn}=\frac{4\mathbf{r}_\alpha+3\mathbf{r}_t+\mathbf{r}_n}{8},$$

where $\mathbf{r}_\alpha=\frac{1}{4}(\mathbf{r}_1+\mathbf{r}_2+\mathbf{r}_3+\mathbf{r}_4)$, $\mathbf{r}_t=\frac{1}{3}(\mathbf{r}_5+\mathbf{r}_6+\mathbf{r}_7)$, and $\mathbf{r}_n=\mathbf{r}_8$ are the center-of-mass coordinates of α, t, and n, respectively. The wave function belonging to this arrangement and to a particular angular momentum set $[(s_1,s_2,s_3)S,(l_1,l_2)L]JM$ reads

$$\Psi^{(\alpha t)n}_{[(s_1,s_2,s_3)S,(l_1,l_2)L]JM}=\sum_K C^{(\alpha t)n}_{K,(s_1,s_2,s_3)S(l_1,l_2)L}\mathscr{A}\{[\Phi_{(s_1,s_2,s_3)S}\Gamma^{(\alpha t)n}_{K(l_1,l_2)L}(\boldsymbol{\rho}_1^{(\alpha t)n},\boldsymbol{\rho}_2^{(\alpha t)n})]_{JM}\}$$

$$=\sum_K C^{(\alpha t)n}_{K,(s_1,s_2,s_3)S(l_1,l_2)L}\mathscr{A}\{[[\phi^\alpha_{s_1}\phi^t_{s_2}\xi^n_{s_3}]_S[\Gamma_{l_1}(\nu^{(\alpha t)n}_{k_1},\boldsymbol{\rho}_1^{(\alpha t)n})\Gamma_{l_2}(\nu^{(\alpha t)n}_{k_2},\boldsymbol{\rho}_2^{(\alpha t)n})]_L]_{JM}\},$$

where $\phi^\alpha_{s_1}$ and $\phi^t_{s_2}$ are the wave functions of the internal motions of α and t, which are costructed from the simplest $0s$ harmonic-oscillator shell model configurations. The spins of the clusters $s_1=0$, $s_2=1/2$, and $s_3=1/2$ are coupled to the total spin S.

APPENDIX B

In this appendix we show the relation of the components of the wave function in different cluster arrangements. The Jacobi coordinates of the $(\alpha n)t$ arrangement have the form

$$\boldsymbol{\rho}_1^{(\alpha n)t}=\mathbf{r}_n-\mathbf{r}_\alpha,$$

$$\boldsymbol{\rho}_2^{(\alpha n)t}=\mathbf{r}_t-\frac{4\mathbf{r}_\alpha+\mathbf{r}_n}{5},$$

$$\mathbf{R}_{\alpha tn}=\frac{4\mathbf{r}_\alpha+3\mathbf{r}_t+\mathbf{r}_n}{8},$$

and the wave function of this arrangement is written as

$$\Psi^{(\alpha n)t}_{[(s_1,s_2,s_3)S,(l_1,l_2)L]JM}=\sum_K C^{(\alpha n)t}_{K,(s_1,s_2,s_3)S(l_1,l_2)L}\mathscr{A}\{[[\phi^\alpha_{s_1}\phi^t_{s_2}\xi^n_{s_3}]_S[\Gamma_{l_1}(\nu^{(\alpha n)t}_{k_1},\boldsymbol{\rho}_1^{(\alpha n)t})\Gamma_{l_2}(\nu^{(\alpha n)t}_{k_2},\boldsymbol{\rho}_2^{(\alpha n)t})]_L]_{JM}\}.$$

The Jacobi coordinates of the arrangements $(\alpha n)t$ and $(\alpha t)n$ are related through the equations

$$\boldsymbol{\rho}_1^{(\alpha n)t}=\frac{3}{7}\boldsymbol{\rho}_1^{(\alpha t)n}+\boldsymbol{\rho}_2^{(\alpha t)n},$$

$$\boldsymbol{\rho}_2^{(\alpha n)t}=\frac{32}{35}\boldsymbol{\rho}_1^{(\alpha t)n}-\frac{1}{5}\boldsymbol{\rho}_2^{(\alpha t)n}.$$

By using these relations and Eq. (1) we can express the Gaussians of the relative motion as

$$[\Gamma_{l_1}(\nu^{(\alpha n)t}_{k_1},\boldsymbol{\rho}_1^{(\alpha n)t})\Gamma_{l_2}(\nu^{(\alpha n)t}_{k_2},\boldsymbol{\rho}_2^{(\alpha n)t})]_{LM}$$

$$=G_{l_1}(\nu^{(\alpha n)t}_{k_1})G_{l_2}(\nu^{(\alpha n)t}_{k_2})e^{-\left[\left(\frac{3}{7}\right)^2\nu^{(\alpha n)t}_{k_1}+\left(\frac{32}{35}\right)^2\nu^{(\alpha n)t}_{k_2}\right](\boldsymbol{\rho}_1^{(\alpha t)n})^2-\left[\nu^{(\alpha n)t}_{k_1}+\left(\frac{1}{5}\right)^2\nu^{(\alpha n)t}_{k_2}\right](\boldsymbol{\rho}_2^{(\alpha t)n})^2-\left(\frac{6}{7}\nu^{(\alpha n)t}_{k_1}-\frac{64}{175}\nu^{(\alpha n)t}_{k_2}\right)\boldsymbol{\rho}_1^{(\alpha t)n}\cdot\boldsymbol{\rho}_2^{(\alpha t)n}}$$

$$\times\left[\mathscr{Y}_{l_1}\left(\frac{3}{7}\boldsymbol{\rho}_1^{(\alpha t)n}+\boldsymbol{\rho}_2^{(\alpha t)n}\right)\mathscr{Y}_{l_2}\left(\frac{32}{35}\boldsymbol{\rho}_1^{(\alpha t)n}-\frac{1}{5}\boldsymbol{\rho}_2^{(\alpha t)n}\right)\right]_{LM}.$$

The above equation shows that the most important consequence of the coordinate transformation is the appearance of a "cross term" $\boldsymbol{\rho}_1^{(\alpha t)n}\cdot\boldsymbol{\rho}_2^{(\alpha t)n}$ in the exponential. This term can be expanded into partial waves as

$$e^{\gamma\boldsymbol{\rho}_1^{(\alpha t)n}\cdot\boldsymbol{\rho}_2^{(\alpha t)n}}=4\pi\sum_{l=0}^{\infty} i_l(\gamma\rho_1^{(\alpha t)n}\rho_1^{(\alpha t)n})\sum_{m=-l}^{l} Y_{lm}(\hat{\boldsymbol{\rho}}_1^{(\alpha t)n})Y_{lm}(\hat{\boldsymbol{\rho}}_2^{(\alpha t)n})^*, \tag{B2}$$

where i_l is the modified spherical Bessel function. The expansion of the product of Gaussians in the $(\alpha n)t$ arrangement [left-hand side (LHS) of Eq. (B1)] in terms of products of Gaussians of the $(\alpha t)n$ arrangement, therefore, requires an infinite summation over the partial waves:

$$[\Gamma_{l_1}(\nu_{k_1}^{(\alpha n)t},\boldsymbol{\rho}_1^{(\alpha n)t})\Gamma_{l_2}(\nu_{k_2}^{(\alpha n)t},\boldsymbol{\rho}_2^{(\alpha n)t})]_{LM}\approx\sum_{K',l_1',l_2'} A_{K',(l_1',l_2')L}[\Gamma_{l_1'}(\nu_{k_1'}^{(\alpha t)n},\boldsymbol{\rho}_1^{(\alpha t)n})\Gamma_{l_2'}(\nu_{k_2'}^{(\alpha t)n},\boldsymbol{\rho}_2^{(\alpha t)n})]_{LM}. \tag{B3}$$

Besides the infinite sum over the partial waves l_1' and l_2', a summation over the various Gaussian size parameters $K'=(k_1',k_2')$ is necessary to approximate the Bessel function. A term of the wave function in the $(\alpha n)t$ arrangement, consequently, can be expressed in the $(\alpha t)n$ arrangement by the infinite sum

$$\mathscr{A}\{[[\phi_{s_1}^{\alpha}\phi_{s_2}^{t}\xi_{s_3}^{n}]_S[\Gamma_{l_1}(\nu_{k_1}^{(\alpha n)t},\boldsymbol{\rho}_1^{(\alpha n)t})\Gamma_{l_2}(\nu_{k_2}^{(\alpha n)t},\boldsymbol{\rho}_2^{(\alpha n)t})]_L]_{JM}\}$$

$$\approx\sum_{K',l_1',l_2'} A_{K',(l_1',l_2')L}\mathscr{A}\{[[\phi_{s_1}^{\alpha}\phi_{s_2}^{t}\xi_{s_3}^{n}]_S[\Gamma_{l_1'}(\nu_{k_1'}^{(\alpha t)n},\boldsymbol{\rho}_1^{(\alpha t)n})\Gamma_{l_2'}(\nu_{k_2'}^{(\alpha t)n},\boldsymbol{\rho}_2^{(\alpha t)n})]_L]_{JM}\}. \tag{B4}$$

The expansion coefficients $A_{K',(l_1',l_2')L}$ depend on the size parameters of the Gaussians of the left- and right-hand sides in Eq. (B4). Some particular choices of these parameters might suppress most of the terms in the sum, leading to a few dominant partial waves. The inclusion of the $(\alpha n)t$ arrangement, therefore, amounts to the inclusion of a certain combination of partial waves of the $(\alpha t)n$ arrangement. In this way, the missing part of the wave function in the $(\alpha t)n$ Jacobi coordinate system (due to the truncation of higher partial waves in this arrangment) is compensated for by the combination of other arrangements.

[1] K. Varga, Y. Suzuki, and R. G. Lovas, Nucl. Phys. **A571**, 447 (1994).
[2] V. I. Kukulin and V. M. Krasnopolsky, J. Phys. G **3**, 795 (1977).
[3] K. Varga, Y. Suzuki, and Y. Ohbayasi, Phys. Rev. C **50**, 189 (1994).
[4] K. Varga and Y. Suzuki, Phys. Rev. C **52**, 2885 (1995).
[5] K. Matsuta, M. Fukuda, M. Tanigaki, T. Minamisono, Y. Nojiri, M. Mihara, T. Onishi, T. Yamaguchi, A. Harada, M. Sasaki, T. Miyake, S. Fukuda, K. Yoshida, A. Ozawa, T. Kobayashi, I. Tanihata, J. R. Alonso, G. F. Krebs, and T. J. M. Symons, contribution to the International Symposium on Physics of Unstable Nuclei, Niigata, 1994 (unpublished).
[6] Y. Fujiwara and Y. C. Tang, Phys. Rev. C **28**, 1869 (1983).
[7] T. Kajino, T. Matsuse, and A. Arima, Nucl. Phys. **A413**, 323 (1984).
[8] T. Mertelmeier and H. M. Hoffman, Nucl. Phys. **A459**, 387 (1986).
[9] H. Kitagawa and H. Sagawa, Phys. Lett. B **299**, 1 (1993).
[10] H. Nakada and T. Otsuka, Phys. Rev. C **49**, 886 (1994).
[11] Y. Fujiwara and Y. C. Tang, Phys. Rev. C **41**, 28 (1990).
[12] D. Baye, P. Descouvemont, and N. K. Timofeyuk, Nucl. Phys. **A577**, 624 (1994).
[13] P. Descouvemont and D. Baye, Phys. Lett. B **292**, 235 (1992).
[14] A. Csótó, Phys. Lett. B **315**, 24 (1993).
[15] Y. Tosaka and Y. Suzuki, Nucl. Phys. **A512**, 46 (1990).
[16] M. V. Zhukov, B. V. Danilin, D. V. Fedorov, J. M. Bang, I. J. Thompson, and J. S. Vaagen, Phys. Rep. **231**, 150 (1993).
[17] H. Kameyama, M. Kamimura, and M. Kawai, in *Proceedings of the International Symposium on Structure and Reactions of Unstable Nuclei*, edited by K. Ikeda and Y. Suzuki (World Scientific, Singapore, 1991).
[18] K. Varga, Comput. Phys. Commun. (to be published).
[19] H. Kamada and W. Glöckle, Nucl. Phys. **A548**, 205 (1992).
[20] M. Kamimura, Phys. Rev. A **38**, 621 (1988).
[21] A. B. Volkov, Nucl. Phys. **74**, 33 (1965).
[22] J. L. Ballot, Z. Phys. A **302**, 347 (1981).
[23] W. H. Press, B. P. Flannery, S. A. Teukolsky, and W. T. Vetterling, *Numerical Recipes in Fortran* (Cambridge University, Cambridge, England, 1992), Chap. 10, p. 406.
[24] I. Reichstein and Y. C. Tang, Nucl. Phys. **A158**, 529 (1970); D. R. Thompson, M. Lemere, and Y. C. Tang, *ibid.* **A286**, 53 (1977).
[25] R. Beck, F. Dickmann, and R. G. Lovas, Ann. Phys. (N.Y.) **173**, 1 (1987).
[26] I. Tanihata, T. Kobayashi, O. Yamakawa, S. Shimoura, K. Ekuni, K. Sugimoto, N. Takahashi, T. Shimoda, and H. Sato, Phys. Lett. B **206**, 592 (1988).
[27] H.-G. Voelk and D. Fick, Nucl. Phys **A530**, 475 (1991).
[28] T. Minamisono, T. Ohtsubo, I. Minami, S. Fukuda, A. Kitagawa, M. Fukuda, K. Matsura, Y. Nojiri, S. Takeda, H. Sagawa, and H. Kitagawa, Phys. Rev. Lett. **69**, 2058 (1992).
[29] E. Arnold *et al.*, Z. Phys. A **331**, 295 (1988).
[30] F. Ajzenberg-Selove, Nucl. Phys. **A490**, 1 (1988).
[31] R. J. Glauber, *Lectures in Theoretical Physics* (Interscience, New York, 1959), Vol. 1, p. 315.
[32] Y. Ogawa, K. Yabana, and Y. Suzuki, Nucl. Phys. **A543**, 722 (1992).

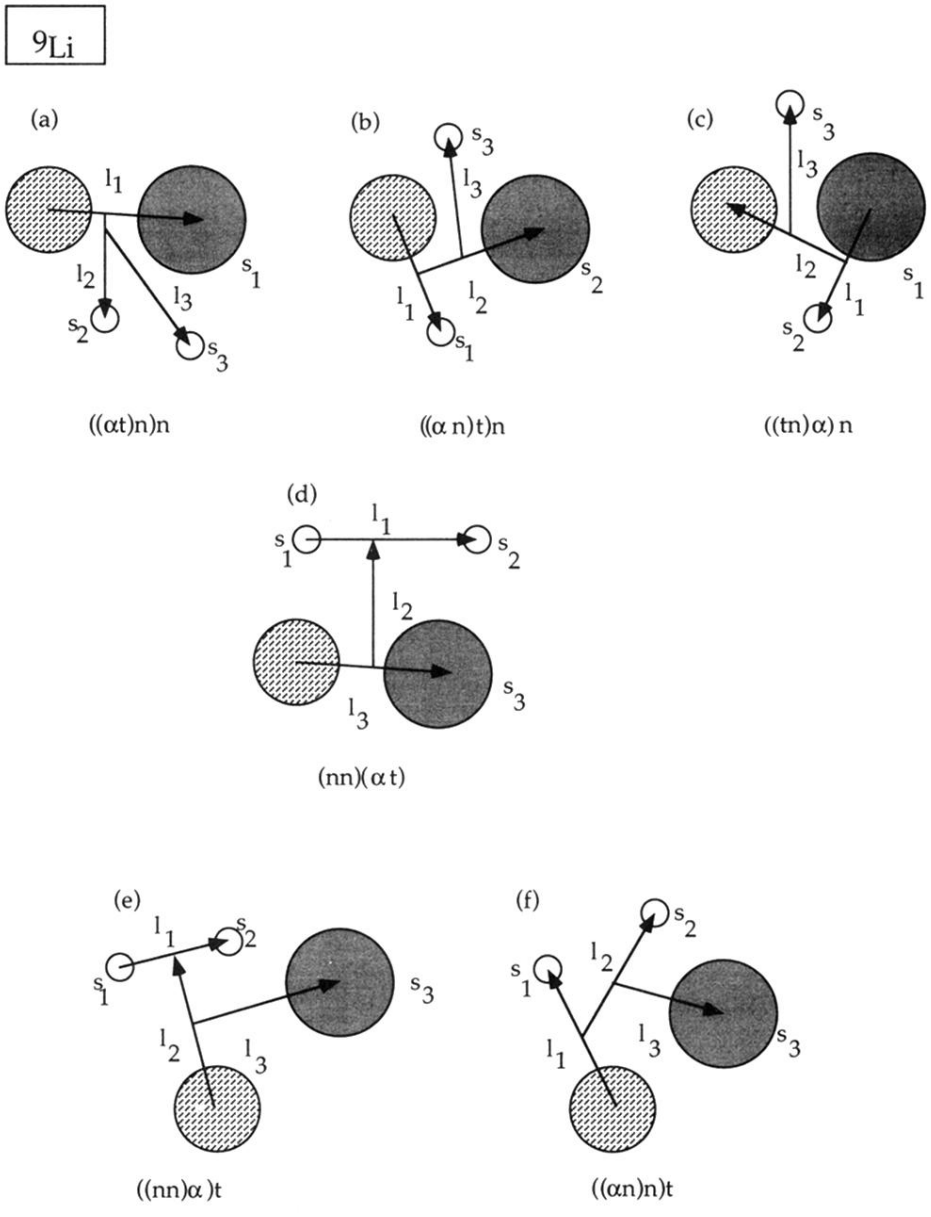

FIG. 1. Different arrangements used in the calculation for ^{9}Li. The small circles are neutrons, the medium-size circle is the alpha particle, and the largest circle is the triton. The orbital angular momenta for the relative motion between the clusters connected by solid line are denoted by l_i. The spin of the clusters is $s_i = 1/2$; the spin of the alpha particle is zero and it is omitted.